Adhesion between a suspended polymeric film and a metallic substrate: Experiments and models

Jing Du and Emily Hampp
Princeton Institute for the Science and Technology of Materials, Princeton University, Princeton, New Jersey 08544; and The Department of Mechanical and Aerospace Engineering, Princeton University, Princeton, New Jersey 08544

Wanliang Shan
Princeton Institute for the Science and Technology of Materials, Princeton University, Princeton, New Jersey 08544; and The Department of Mechanical and Aerospace Engineering, Princeton University, Princeton, New Jersey 08544; and Cordis Corporation, a Johnson & Johnson Company, Spring House, Pennsylvania 19477

Hannah Li, George Papandreou, and Cynthia A. Maryanoff
Cordis Corporation, a Johnson & Johnson Company, Spring House, Pennsylvania 19477

Winston O. Soboyejo[a)]
Princeton Institute for the Science and Technology of Materials, Princeton University, Princeton, New Jersey, 08544; and The Department of Mechanical and Aerospace Engineering, Princeton University, Princeton, New Jersey 08544; and Department of Materials Science and Engineering, The African University of Science and Technology, Abuja, Federal Capital Territory, Nigeria

(Received 25 February 2012; accepted 10 May 2012)

This paper presents the results of a combined experimental, theoretical, and computational study of the adhesion between suspended polymeric films and a substrate in a model drug-eluting stent. Atomic force microscope is used to measure the pull-off force between the polymer and the substrate. The adhesion energy was then obtained from the measured pull-off forces and adhesion theories. Subsequently, the adhesion energy was incorporated into interfacial fracture mechanics zone model that was used to determine mode mixity dependence of the interfacial fracture toughness. The mode mixity-dependent fracture toughness conditions were then integrated into finite element models that were used to compute the critical push-out force of the suspended polymeric films. The predicted push-out forces were in good agreement with the results obtained from the experiments.

I. INTRODUCTION

In earlier work,[1–3] we presented a range of atomic force microscopy and fracture mechanics techniques for the measurement of adhesion and interfacial fracture toughness for the polymeric films on hard substrates. The methods were applied largely to the characterization of adhesion in drug-eluting stents (DESs) with thin-film drug coatings on their surfaces. The first generation of such systems had thin conformal coatings in direct contact with the underlying metallic scaffold. For example, the CYPHER® Sirolimus-eluting Coronary Stent[3] (Cordis, Springhouse, PA) consists of a coating of a Parylene-C primer layer, and a drug-eluting layer of sirolimus, poly(n-butyl methacrylate), and poly (ethylene-co-vinyl acetate) on 316L stainless steel scaffold.

In an effort to evaluate adhesion between the layers of the coating, and also between the coating and the substrate, surface pairs were identified to represent both the individual components and the complete chemistry of each layer. Coated atomic force microscope (AFM) tips and two-dimensional coupons, which act as surrogates to the substrate, were prepared and characterized. Force measurements were then obtained to evaluate the adhesion between all the possible interfaces within the coating and between the coating and the substrate.

The interfacial fracture energy release rate, G, was also calculated with the application of the adhesion and fracture mechanics models. The predictions from the models were then validated using independent Brazil disk tests that were conducted on model specimens that contained interfaces that mimic those between the layers in the coating. The measurements of interfacial fracture toughness were then obtained over a range of mode mixities that range from pure mode I and mode II.

In this work, we extend our efforts to the case of suspended films with partial contact with their substrates (Fig. 1). This investigation is based on a model NEVO™ Sirolimus-eluting Coronary Stent (NEVO™ SES; Cordis Corporation, Warren, NJ) consisting of a formulation of sirolimus drug and a degradable polymer poly(D,L-lactide-co-glycolide) (PLGA), suspended within several hundred L605 Co–Cr alloy reservoirs (length 120 μm × width 80 μm × depth 100 μm).

[a)]Address all correspondence to this author.
e-mail: soboyejo@princeton.edu
DOI: 10.1557/jmr.2012.178

 © Materials Research Society 2012

https://doi.org/10.1557/jmr.2012.178 Published online by Cambridge University Press

Shan et al.[4] have described the development of a novel push-out test to measure the adhesion force between the suspended polymeric films and the substrate, as well as the cohesion force within the films. However, the interfacial fracture energy release rate was not obtained in the earlier study by Shan et al.[4]

This paper uses AFM to evaluate the intermolecular adhesion energy between the suspended film and stent of the NEVO™ SES. A combination of adhesion and fracture mechanics theories is then used to estimate interfacial fracture. The effects of mode mixity are then modeled using a zone-shielding model. The results are incorporated into finite element simulation of drug push-out tests. The simulations are in good agreement with experimental force measurements obtained from drug push-out tests.

II. MODELING

A. AFM force measurements and tip calibration

The steps of AFM adhesion measurements are summarized in Fig. 2.[5] First, the AFM tips were dip coated before lowering them toward the substrate surface at a constant velocity [Fig. 2(a)]. As the probe approaches the surface under ambient conditions, the tip experiences negligible interactions with the surrounding medium and the tip deflection remains close to zero. However, as the tip is lowered further down, it is eventually pulled into contact with the surface by adhesive force interactions [Fig. 2(b)] between the tip of the probe and the substrate. Subsequently, the scanner continues to move down but with the substrate and probe in continuous contact. This causes the tip to bend [Fig. 2(c)] under elastic deformation. Upon reversal of the direction of tip displacement, the scanner head is raised and the tip's elastic deformation is reversed. However, residual adhesive interactions prevent the tip from detaching from the substrate's surface at zero loads [Fig. 2(d)]. Hence, the reversed loading of the tip must be continued until the adhesive forces are eventually overcome at a negative force that corresponds to the pull-off force [Fig. 2(e)]. The measured displacement deflection can then be related to the adhesion force via Hooke's law. This gives

$$F = kx \quad , \tag{1}$$

where k is the spring constant and x is the tip displacement. However, the accuracy of the AFM measurements of the adhesion force depends significantly on the careful measurement of the spring constant, k, of the AFM cantilever tip.

Although the values for the spring constant are provided by most tip manufacturers, these are batch estimates that are often significantly different from the actual values for each tip. Hence, the thermal tune method[6] provides a real-time and accurate method for the measurement of spring constants. It measures the tip response in the presence of thermal agitations and then uses a Lorentzian line shape fit to obtain an accurate estimate of the spring constant from the resulting frequency spectrum of harmonic oscillations.

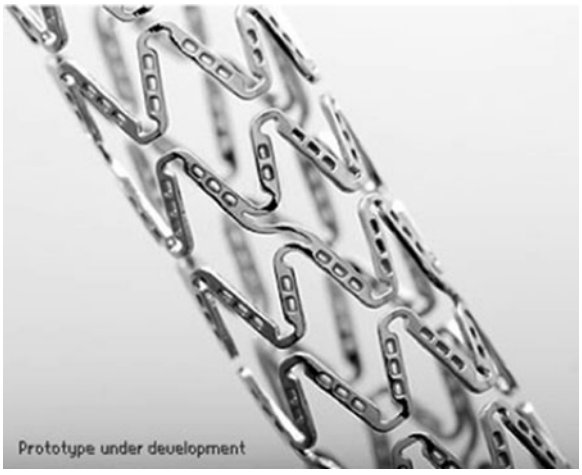


FIG. 1. Optical microscopy image of NEVO™ SES.

B. Adhesion energy theories

This section presents a review of theories that have been proposed for the characterization of the adhesive interactions.[7–9] The Johnson–Kendall–Roberts (JKR) model[7] describes the contact between soft materials with

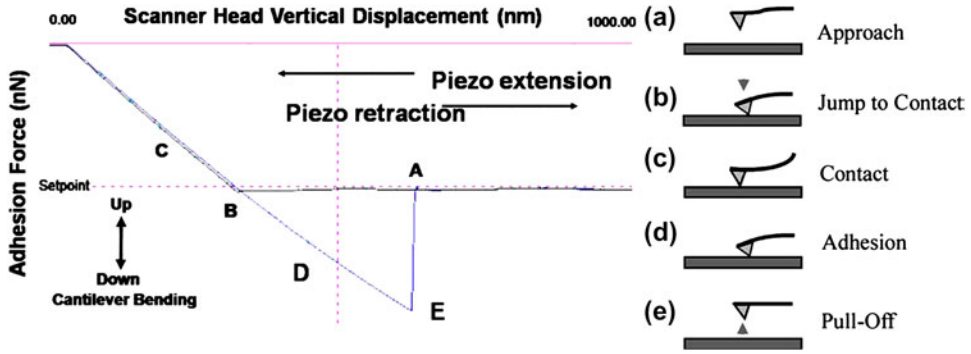


FIG. 2. Schematics illustrating AFM pull-off force measurement.[5]

https://doi.org/10.1557/jmr.2012.178 Published online by Cambridge University Press

short range, strong adhesion forces, and large tip radii. It gives the adhesion energy as:

$$\gamma_{JKR} = \frac{2F}{3\pi R} \quad . \tag{2}$$

In contrast, the Derjaguin–Muller–Toporov (DMT) model[8] applies to adhesion between stiff materials with long range, weak adhesion forces, and small tip radii. It gives the adhesion energy as:

$$\gamma_{DMT} = \frac{F}{2\pi R} \quad . \tag{3}$$

Intermediate between the JKR and DMT models, the Maugis–Dugdale (MD) model[9] proposes an analytical solution. To select the appropriate model, the transition parameter, λ, is defined by[9]:

$$\lambda = 2\sigma_0 \left(\frac{R}{\pi K^2 \gamma} \right)^{1/3} \quad , \tag{4}$$

where γ is the adhesion energy per unit area; R is the combined radius given by $R = R_1R_2/(R_1 + R_2)$, where R_1 and R_2 are the radii of the two spheres, respectively; K is the combined elastic modulus for two spheres in contact, which is given by $K = 4/3[(1-\nu_1)^2/E_1 + (1-\nu_2)^2/E_2]^{-1}$, where E_1 and E_2 are the elastic moduli of the two spheres and ν_1 and ν_2 are the Poisson ratios of the two spheres, respectively. σ_0 is assumed to be a constant adhesive stress that acts over a displacement range of δ_t, which gives the adhesion energy as $\gamma = \sigma_0\delta_t$. By choosing σ_0 to match the minimum adhesive stress of a Lennard–Jones potential with equilibrium separation distance z_0, it follows that $\delta_t = 0.97z_0$. The JKR model applies when $\lambda > 5$. The DMT model applies when $\lambda < 0.1$. The MD model applies for the intermediate values of λ.

C. Interfacial failure zone model

Although the adhesion theories described above can be used to estimate the interfacial energy corresponding to mode I fracture, they do not capture the shielding effects that occur due to nonplanar asperity contacts at mode mixities greater than zero.[2,3,10] Such effects can be modeled using an idealized geometry corresponding to contacts in the zone model[11] shown schematically in Fig. 3. Here, l is the spacing between microcracks, D is the facet length, H is the facet height, and L is the contact zone size. Note that the model neglects friction. It is also assumed that, within the contact zone, the shear stresses and displacements are elastic and analogous to those associated with a linear array of microcracks or an equivalent array of bridges.[12] The mode mixity ψ is defined by the phase angle of loading, such that $\tan\psi = K_{II}/K_I$, where K_I and K_{II} are the stress intensity factor of mode I and mode II, respectively. The crack tip shielding is thus given by[11]:

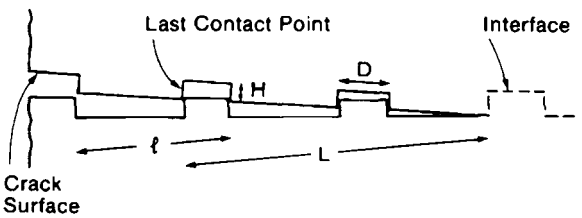


FIG. 3. Zone configuration for zone model.[11]

$$\frac{\Delta G}{G} = \frac{\tan^2\psi(1 - k[\alpha_0(1+\tan^2\psi)(\Delta G/G + 1)])}{1+\tan^2\psi} \quad , \tag{5}$$

where ΔG is the reduction in crack energy release rate, i.e., the shielding, caused by the contact locking of facet, $\alpha_0 = \pi(EH^2/lG_0)/[32(1-\nu^2)\ln(1/\sin(\pi D/2l))]$ is a material property parameter, E is Young's modulus, ν is the Poisson ratio, and k is a function of α defined by Evans and Hutchinson.[11]

D. Finite element modeling

In the suspended film push-out tests, a tungsten probe was used to apply the load on thin suspended films surrounded by hard substrates. Finite element modeling was performed using the ABAQUS software package (Dassault Systemes Simulia Corporation, Providence, RI). This was used to simulate the push-out test process. It was also used to calculate the critical force required for adhesive failure between the suspended films and reservoirs.

For simplification, an axisymmetric model was built, as shown in Fig. 4. In this model, the probe was approximated as cylinder, while the reservoir was approximated as a hollow cylinder that contains the polymer film. The geometry of the stent was based on simplified geometries of NEVO™ SES. The geometry of the probe tip was based on the simplified geometry of the probe used in the push-out test.

The model assumed that the materials of the probe and stent exhibited isotropic elastic behavior. Many polymeric materials have the hyperelastic material behavior. Unfortunately, there were not enough required data for the modeling of the hyperelastic material behavior for the material of the polymeric inlay. Also, experiments[13] showed that the elongation of PLGA at failure is only 5.7%, which makes it unlikely a hyperelastic material. It was assumed here that the material of the polymeric inlay exhibited elastic–perfectly plastic behavior, with mechanical properties that are summarized in Table I. Note that, considering the unknown effects of mixing of the drug and the PLGA polymer, the Young's modulus of the formulation was taken as that of the PLGA. The axisymmetric boundary condition was applied

https://doi.org/10.1557/jmr.2012.178 Published online by Cambridge University Press

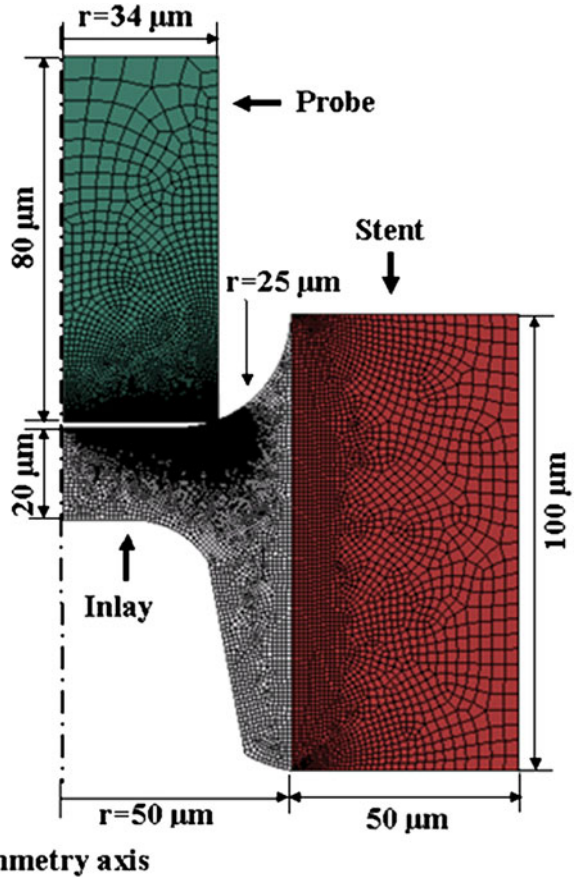


FIG. 4. Finite element model of the NEVO™ SES inlay push-out process.

TABLE I. Mechanical properties used in the finite element modeling.

Materials	Young's modulus	Poisson's ratio	Yielding stress
Tungsten	410 GPa[15]	0.28[15]	...
Co–Cr	243 GPa[16]	0.3	...
PLGA 75/25	629.3 MPa[13]	0.3	26.6 MPa[13]

at the symmetry axis, as shown in Fig. 4. Also, the outside edge of the stent was fixed to have no displacements and rotations. Vertical displacement was applied to the top of the probe.

The model was meshed with linear four-node axisymmetric elements. The mesh was refined at the probe/inlay contact region to accommodate the relatively large deformation. The inlay/reservoir interface was meshed with nodes shared by the neighboring elements in the inlay and the reservoir. As illustrated in Fig. 5, the surface interaction at the inlay/reservoir interface was modeled as a nonlinear spring array, characterized by a tensile and a shear traction–separation law. Before the damage initiates, linear elastic behavior is assumed. However, after the damage initiates, the failure of the interface is characterized by the progressive degradation of the spring stiffness.

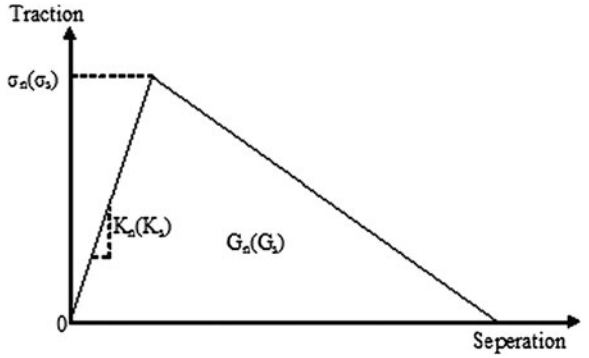


FIG. 5. A schematic of the traction–separation laws used to model the inlay/reservoir interface.

The model, shown schematically in Fig. 5, can be described by six parameters. These include: the interfacial tensile strength σ_n and shear strength σ_s, corresponding opening and sliding spring constants K_n and K_s, and the areas under the traction–separation curves G_n and G_s, which are the fracture energies needed to damage the interface.

Based on von Mises yield criterion, the relation between tensile yield stress σ_y and shear yield stress τ_y could be described by $\tau_y = \sigma_y/\sqrt{3}$. Accordingly, the traction–separation law parameters σ_n and σ_s were selected to have $\sigma_s = \sigma_n/\sqrt{3}$. For isotropic linear elastic materials, Young's modulus E and the shear modulus G could be related by $E = 2G(1 + \nu)$. Similarly, the traction–separation law parameters K_n and K_s were selected to have $K_n = 2K_s(1 + \nu)$. The parameters chosen for the simulation were listed in Table II.

A mixed mode damage evolution behavior is described by choosing the area under the traction–separation curve as the energy release rate derived from the zone model[11] for each corresponding mode mixity, such that G_n and G_s equal to mode I and mode II critical energy release rate, respectively.

The effective separation δ is defined by $\delta = \sqrt{\delta_n^2 + \delta_s^2}$. Considering the mixed mode energy failure criterion, the effective failure separation δ^f could be defined by $\delta^f = 2G_c/\sigma^0$, where G_c is the critical energy release rate and σ^0 is the effective traction at damage initiation. The evolution of the interface damage could be described by a scalar damage variable as

$$D = \frac{\delta^f(\delta^{\max} - \delta^0)}{\delta^{\max}(\delta^f - \delta^0)} \quad , \tag{6}$$

where $\delta^{\max}$ is the maximum value of the effective separation during the loading history and the δ^0 is the effective separation when the damage initiates. The damage variable D is 0 when damage initiates. The damage variable also increases monotonically upon further loading and finally reaches a value of 1 when G_c is reached.

https://doi.org/10.1557/jmr.2012.178 Published online by Cambridge University Press

III. EXPERIMENTAL PROCEDURES

A. AFM experiments

MPP-31100-W-rotated silicon tips (Bruker Nano, Santa Barbara, CA) were used in the experiments. They were selected from the same wafer to reduce possible batch effects. They were then coated with a solution of sirolimus and the degradable polymer PLGA, applying the inlay chemistry of the NEVO™ SES by dip-coating method used in the prior work.[1,3] After coating, scanning electron microscopy (SEM) images were obtained along with energy dispersive spectroscopy (EDS) analysis in a FEI XL30 FEG-SEM (Philips, Hillsboro, OR). The same SEM was also used to measure the AFM tip radii.

Electropolished L605 Co–Cr coupons with dimensions $48 \times 14 \times 0.5$ mm were used as substrates. They are made of the same material used to produce the NEVO™ SES and have similar surface characteristics. A Wyco NT 3300 optical profiler (Veeco Instruments, Tucson, AZ) was used to perform white light interferometry that was used to characterize the surface roughness of the coupons at three different spots on the coupon. The measured surface roughnesses and tip radii were then used to calculate the combined radius.

A Dimension 3000 AFM (Digital Instruments, Plainview, NY) was used to perform contact AFM measurements in air, over a temperature range of 20–25 °C and relative humidity range of 36–45%. About five to six force measurements were conducted on each spot of the substrate. In total, three spots were tested, which gave a total of 17 force curves. The spring constant of each tip was measured using the thermal tune method with a Nanoscope IIIa AFM (Digital Instruments). By substituting the spring constant and the measured displacements into Eq. (1), the pull-off forces were estimated for the interface between the polymer coated tips and the L605 Co–Cr substrates.

B. Suspended films push-out test

Following the methods described in Shan et al.,[4] suspended film push-out tests were carried out on the NEVO™ SES (Cordis Corporation) using a tungsten probe with a rectangular cross section of 45×90 μm. The specimens were expanded, taken off the catheter, then cut, flattened, and clamped immediately after opening the package. They were then tested within 3 h of exposure to the lab environment (38–55% relative humidity and 20–25 °C temperature). The critical forces required to detach the suspended inlays from the force–time measurements and the in situ observations of drug push out. The samples were also examined in an environmental EVO SEM (Carl Zeiss NTS, LLC, Peabody, MA) after the push-out tests. This was done to confirm the push out of the suspended drug layers. The SEM imaging was also combined with EDS analysis, which was used to confirm the occurrence of adhesive failure.

TABLE II. Parameters for the traction–separation model.

Parameter	K (N/m^3)	σ (MPa)	G (J/m^2)
Normal direction	104	5.5	0.23
Shear direction	40	3.2	0.76

IV. RESULTS AND DISCUSSION

A. Adhesion force measurements and surface energy

The tip radii of the NEVO™ SES formulation-coated tips were measured to be 561 ± 36 nm from three SEM images. A typical coated tip is shown in Fig. 6. The corresponding EDS spectrum (Fig. 7) also confirmed that an organic coating was presented on the tip, resulting in a higher concentration of carbon and oxygen. The surface roughness of L605 Co–Cr coupons was measured on three samples by white light interferometry to be 188 ± 7 nm. The surface morphology image of one of the measured spots is presented in Fig. 8. The pull-off force measured by AFM was 151 ± 74 nN. The adhesion energy was calculated for both JKR model[7] and DMT model[8] using Eqs. (2) and (3), respectively.

In the case of the NEVO™ inlay/reservoir interface examined in this work, the material properties of polymer and L605 alloy are presented in Table I. Using the values presented in the table, the λ parameter was calculated from Eq. (4) to be 18.2 ± 6.5. Since this is greater than 5, the adhesion was modeled using JKR theory.[7] This was also consistent with the AFM force–displacement plots that showed only short-range adhesive interactions between the NEVO™ formulation-coated tips and the L605 Co–Cr coupons (Fig. 9). The adhesion energy calculated by the JKR model was 0.23 ± 0.11 J/m^2. This value is comparable

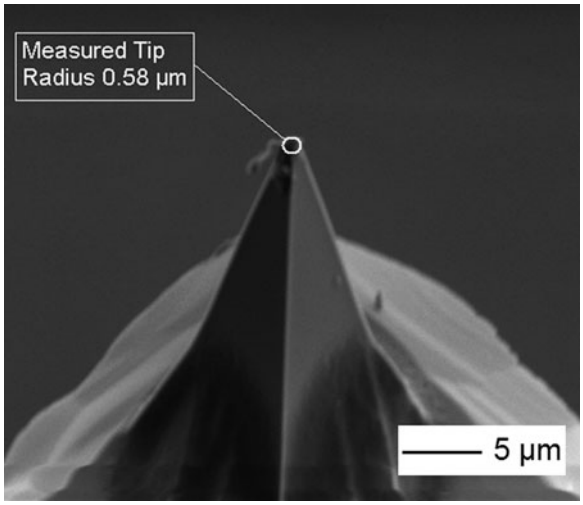


FIG. 6. Sample SEM image of coated AFM tip profile.

https://doi.org/10.1557/jmr.2012.178 Published online by Cambridge University Press

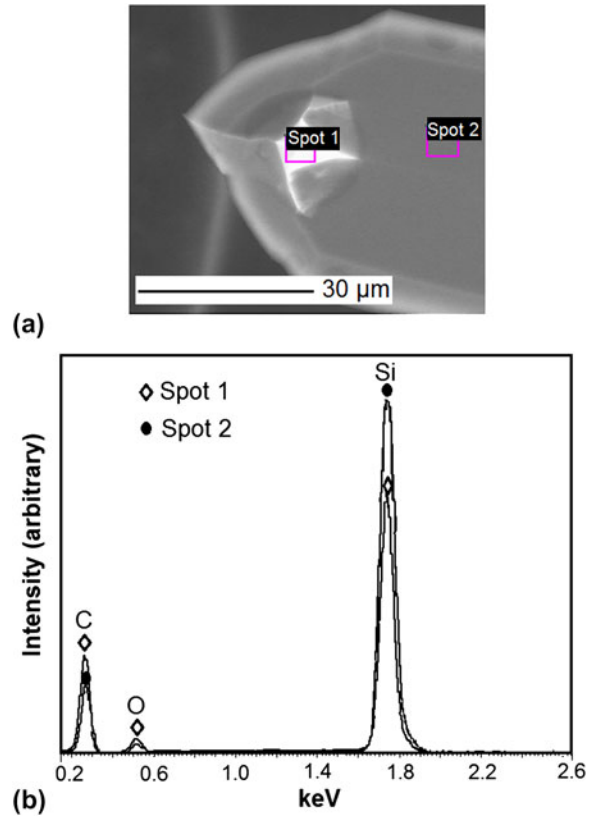


FIG. 7. EDS Spectrum of NEVO™ formulation-coated AFM tips. (a) SEM image of two measured spots. Spot 1 is NEVO™ SES formulation-coated tip; Spot 2 is the clean cantilever. (b) EDS spectra of two measured spots.

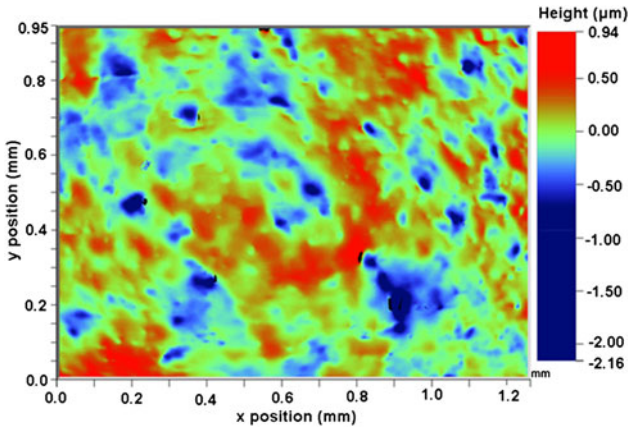


FIG. 8. Surface profile of the L605 Co–Cr alloy coupon.

to the adhesion energy between parylene C and 316L stainless steel measured by Rahbar et al.,[2] which is also an interaction between polymer and metal.

B. Interfacial failure zone model

The surface morphology of the NEVO™ SES stents (away from the reservoirs) was evaluated by profilometry

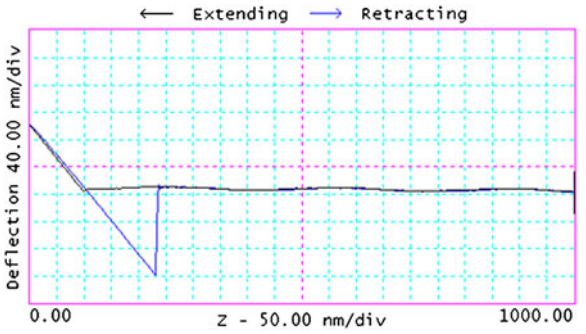


FIG. 9. Typical force–displacement curve obtained for AFM force measurement between NEVO™ formulation and L605 Co–Cr alloy.

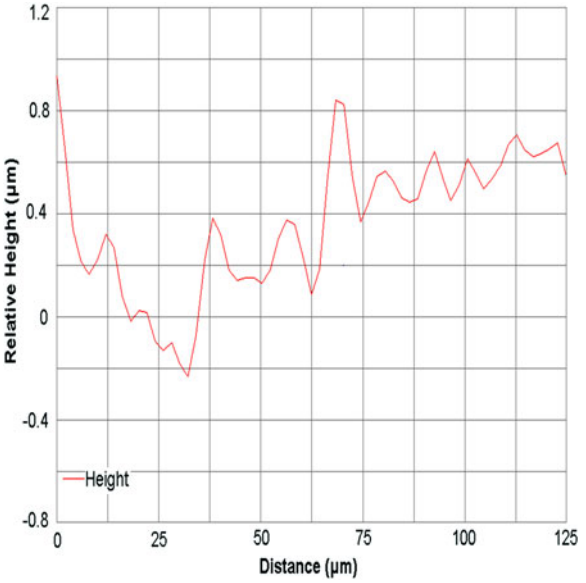


FIG. 10. Surface profile of NEVO™ SES stents away from the reservoirs.

using a P15 Surface Profiler (KLA-Tencor, Milpitas, CA). A typical plot of the stent surface profile is shown in Fig. 10. Assuming that each microcrack in the side profiles in Fig. 3 corresponds to the asperities obtained from the profilometry image presented in Fig. 10, the interfacial crack geometry parameters for zone model were evaluated using this surface profile. The spacing between microcracks, l, was measured to be ~10 μm; the facet length, D, was ~5 μm; and the facet height, H, was 0.2 μm. The materials parameter σ_0 was then calculated to be 1.30×10^{-3}.

The values of crack-tip shielding $\Delta G/G$ for different mode mixities were extracted from the plot by Evans and Hutchinson.[11] Considering that the adhesion energy, γ, obtained from AFM force measurements as the intrinsic mode I fracture toughness, mode mixity dependence predicted by Eq. (5) is presented in Fig. 11. The increase in the

https://doi.org/10.1557/jmr.2012.178 Published online by Cambridge University Press

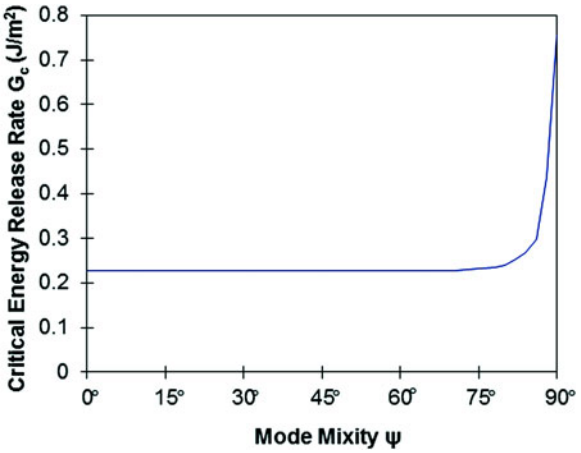


FIG. 11. Variation in critical energy release rate G_c with phase angle of loading.

fracture toughness with increasing mode mixity was due to crack-tip shielding and facet locking phenomena.

C. Suspended films push-out tests

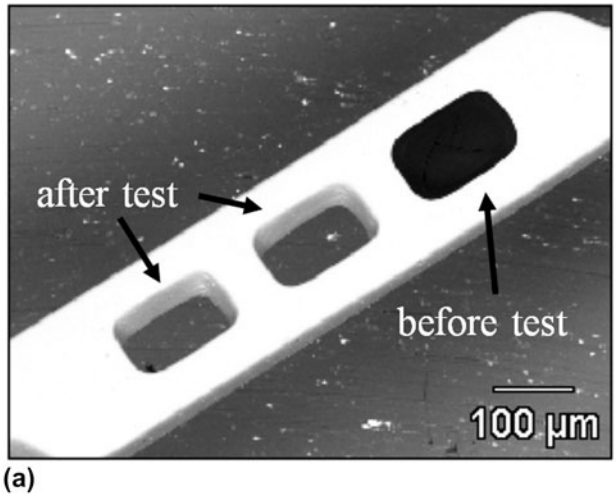
Suspended films push-out tests were performed on a total of 10 inlays of the NEVO™ SES. A typical SEM image is presented in Fig. 12(a). Also, the EDS map shown in Fig. 12(b) confirms that fracture occurred at the interface between the drug inlay and the reservoir. It is important to note here that the observed adhesion failure mode was partly due to the selection of probe tip size, which was designed to promote adhesion failure. Also, the measured critical push-out force F_c was determined to be 81.2 ± 20.2 mN. The interface adhesion shear strength was defined by

$$\tau_c = F_c/cH \quad , \tag{7}$$

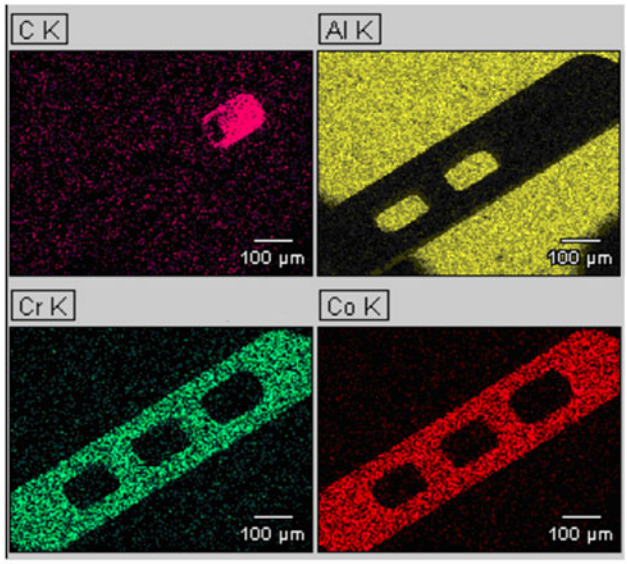
where c and H are the circumference and the height of the inlay, respectively. By taking $H = 100$ μm and $c = 400$ μm, the shear strength of the inlay/reservoir interface was calculated to be 2.0 ± 0.5 MPa. This lower adhesive strength value is attributed to the fact that the adhesive failure corresponds to a condition in which a debond has extended across the interface. Hence, this represents a lower bound measurement of stress required to overcome adhesive interactions, sliding friction, and residual stress effects.[14]

D. Finite element modeling of push-out tests

In the finite element modeling of NEVO™ SES push-out test, the probe moved down gradually to push out the inlay. The push-out force, i.e., the reaction force at the probe, was determined from the force–displacement curves obtained from the finite element simulations. Our simulations showed that the slope of the push-out force–displacement curve



(a)



(b)

FIG. 12. SEM images and EDS mapping of NEVO™ SES after push-out test, demonstrating adhesive failure mode. (a) SEM images. (b) EDS mapping.

depended on the combined effect of inlay stiffness and inlay/reservoir interface stiffness [Fig. 13(a)].

The critical force mostly depended on the strength of inlay/reservoir interface, while the other parameters of the traction–separation interface property are of secondary importance to the critical force [Fig. 13(a)]. The area of the push-out force–displacement curve depended on both the plasticity of the inlay and the area of the traction–separation curve, i.e., the critical energy release rate.

The computed push-out force–displacement curve for an interface with a shear strength of 3.2 MPa is presented in Fig. 13(a). The critical push-out force was calculated to be 72.1 mN. This is in good agreement with the measured values of 81.2 ± 20.2 mN obtained from the push-out tests on the NEVO™ SES. Since there were not enough data

https://doi.org/10.1557/jmr.2012.178 Published online by Cambridge University Press

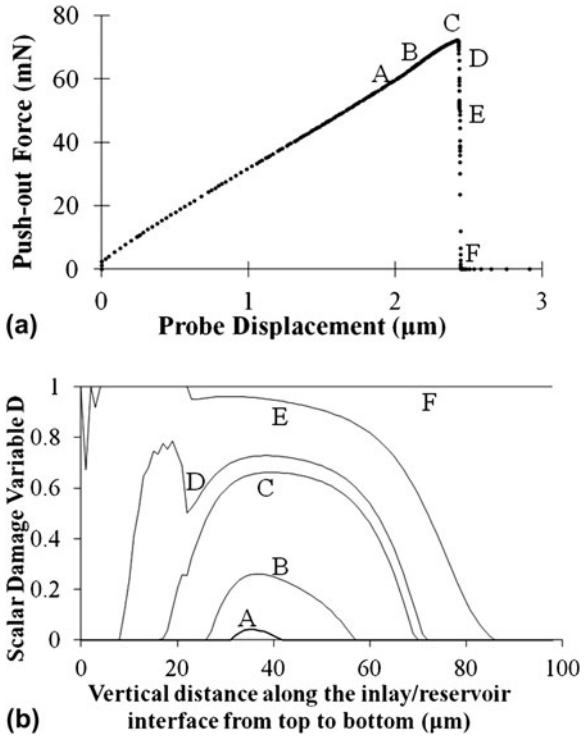


FIG. 13. Push-out force and damage variable calculated by finite element modeling. (a) Push-out force. (b) Damage variable.

points obtained for each condition, it is unlikely that the current results are sufficient for probabilistic analysis. Nevertheless, probabilistic analysis in the future could be useful to show evidence of statistical variance in the experimental results.

The damage variable, D, obtained at several points along the interface, is plotted in Fig. 13(b). This shows that the damage initiated in the middle of the inlay/reservoir interface but evolved more rapidly in the upper part of the interface, as a combined effect of tensile and shear separation. The crack initiated along the upper section of the interface and propagated across the interface.

It is important to note here that the interfacial shear strength that was used in the finite element method (FEM) was greater than the value calculated from Eq. (7). This is because the onset of final failure corresponded to a partially debonded interface, as shown in the damage variable at the critical point in Fig. 13(b). Also, the plasticity of the inlay, which was also considered in the FEM analyses, contributed to the higher value of the interface shear strength.

V. SUMMARY AND CONCLUDING REMARKS

This paper presents the results of a combined experimental, theoretical, and computational study of adhesion and interfacial fracture between a suspended film and a stent substrate in a model DES. The adhesion force was measured using force microscopy during AFM. A combination of adhesion theories and fracture mechanics concepts was then used to estimate the mode mixity dependence of the critical interfacial energy release rates. These were incorporated into a finite element model that was used to simulate the deformation and interfacial cracking processes between the suspended formulation inlay and the stent substrate. The predicted critical forces and load–displacement behavior were in good agreement with experimental results obtained from the suspended polymeric film push-out tests.

ACKNOWLEDGMENTS

The research was supported by the Cordis Corporation, a Johnson & Johnson Company, the NSF MRSEC program through the Princeton Center for Complex Materials (Grant DMR-0819860) and the Grand Challenges Program at Princeton University. The authors are grateful to Prof. Zhigang Suo of Harvard University, for useful technical discussions. We are also grateful to Dr. Nan Yao, Dr. Gerald R. Poirier, and Mr. Joe Palmer for their technical assistance.

REFERENCES

1. K.V. Wolf, Z. Zong, J. Meng, A. Orana, N. Rahbar, K.M. Balss, G. Papandreou, C.A. Maryanoff, and W.O. Soboyejo: An investigation of adhesion in drug-eluting stent layers. *J. Biomed. Mater. Res. Part A* **87**, 272–281 (2008).
2. N. Rahbar, K. Wolf, A. Orana, R. Fennimore, Z. Zong, J. Meng, G. Papandreou, C. Maryanoff, and W. Soboyejo: Adhesion and interfacial fracture toughness between hard and soft materials. *J. Appl. Phys.* **104**, 103533 (2008).
3. J. Meng, A. Orana, T. Tan, K. Wolf, N. Rahbar, H. Li, G. Papandreou, C. Maryanoff, and W. Soboyejo: Adhesion and interfacial fracture in drug-eluting stents. *J. Mater. Res.* **25**, 641 (2010).
4. W. Shan, J. Du, E. Hampp, H. Li, G. Papandreou, C.A. Maryanoff, and W.O. Soboyejo: Adhesion and cohesion in structures containing suspended microscopic polymeric films. *Acta Biomater.* **4**, 1469 (2012).
5. Digital Instruments: *Force Imaging: Support Note No. 228, Rev. E.* (Digital Instruments, Veeco Metrology, Santa Barbara, CA, 1999).
6. F.M. Serry: *Improving the Accuracy of AFM Force Measurements: The Thermal Tune Solution to the Cantilever Spring Constant Problem* (Veeco Instruments Inc., Santa Barbara, CA, 2005).
7. K.L. Johnson, K. Kendall, and A.D. Roberts: Surface energy and the contact of elastic solids. *Proc. R. Soc. London, Ser. A* **324**, 301 (1971).
8. B. Derjaguin: Effect of contact deformations on the adhesion of particles. *J. Colloid Interface Sci.* **53**, 314 (1975).
9. D. Maugis: Adhesion of spheres: The JKR-DMT transition using a Dugdale model. *J. Colloid Interface Sci.* **150**, 243 (1992).
10. R. Venkatesh: Mechanical properties of alumina fiber/glass matrix composites with and without a tin dioxide interface. *Mater. Sci. Eng., A* **268**, 47 (1999).
11. A. Evans and J. Hutchinson: Effects of non-planarity on the mixed mode fracture resistance of bimaterial interfaces. *Acta Metall.* **37**, 909–916 (1989).
12. B. Budiansky, J.C. Amazigo, and A.G. Evans: Small-scale crack bridging and the fracture toughness of particulate-reinforced ceramics. *J. Mech. Phys. Solids* **36**, 167 (1988).

https://doi.org/10.1557/jmr.2012.178 Published online by Cambridge University Press

13. S.H. Choi and T.G. Park: Synthesis and characterization of elastic PLGA/PCL/PLGA tri-block copolymers. *J. Biomater. Sci., Polym. Ed.* **13**, 1163 (2002).
14. C-H. Hsueh: Interfacial debonding and fiber pull-out stresses of fiber-reinforced composites IV: Sliding due to residual stresses. *Mater. Sci. Eng., A* **145**, 143 (1991).
15. R.D. Conner, R.B. Dandliker, and W.L. Johnson: Mechanical properties of tungsten and steel fiber reinforced $Zr_{41.25}Ti_{13.75}Cu_{12.5}Ni_{10}Be_{22.5}$ metallic glass matrix composites. *Acta Mater.* **46**, 6089 (1998).
16. R.V. Marrey, R. Burgermeister, R.B. Grishaber, and R.O. Ritchie: Fatigue and life prediction for cobalt-chromium stents: A fracture mechanics analysis. *Biomaterials* **27**, 1988 (2006).

https://doi.org/10.1557/jmr.2012.178 Published online by Cambridge University Press